


Modeling the hydraulic conductivity of two soils amended with biochars using a statistical-physical model**

Bogusław Usowicz^{1,2} , Jerzy Lipiec¹ *

¹Institute of Agrophysics, Polish Academy of Sciences, Doświadczalna 4, 20-290 Lublin, Poland

²Faculty of Civil Engineering and Environmental Sciences, Białystok University of Technology, Wiejska 45 E, 15-351 Białystok, Poland

Received March 25, 2025; accepted May 26, 2025

Abstract. This study aimed to predict the effect of biochars (from woodchips, rice straw, and manure processed at temperatures from 300 to 700°C) on hydraulic conductivity, volumes of variously sized capillaries (from 360.4 to 0.24 μm radius), and equivalent capillary length of sandy and loamy soils using the statistical-physical model. The model analyzes the connections between soil and biochar and spaces occupied by water and air. The biochars decreased the predicted hydraulic conductivity at the matric potentials from -1 to around -70 cm H_2O by 9 to 25% and increased by 1.6 to 19% at a drier range of potential from around -500 to $-15\,000$ cm H_2O in the sandy soil and increased in the loamy soil across the whole potential range. The greatest effect on the hydraulic conductivity had biochars from the rice straw in sandy soil and woodchips in loamy soil. The biochars generally increased the volumes of all capillaries in the sandy soil. They decreased the volumes of larger capillaries (360.4–3.6 μm radius) and increased that of capillaries of 0.53 μm radius in the loamy soil. All biochars typically decreased the equivalent capillary length in the sandy soil and increased in the loamy soil.

Keywords: organic soil conditioners, unsaturated hydraulic conductivity, capillary size distribution, soil texture, predictive model performance

1. INTRODUCTION

Effectively using water resources in irrigated and rain-fed agriculture requires a comprehensive understanding of the soil's hydraulic properties (Każmierowski, 2015; Saeidi

et al., 2023; Faloye *et al.*, 2024). Data on saturated hydraulic conductivity (K_{sat}) and unsaturated hydraulic conductivity as a function of soil water status govern the water flow and provide information on the rate at which water infiltrates soil water and moves to plant roots (Kirkham, 2005; Gliński and Lipiec, 2018; Orzechowski *et al.*, 2022). The soil's hydraulic conductivity is affected by the inherent soil texture, the genetic type (Kelishadi *et al.*, 2014; Azadmard *et al.*, 2018, 2020; Edeh *et al.*, 2020; Usowicz *et al.*, 2024), and the related pore structure (Faloye *et al.*, 2024). Besides, soil's hydraulic properties can be altered by human activities (Lipiec *et al.*, 2021; Hessel *et al.*, 2022), including the application of biochar (Ajayi *et al.*, 2016; Chen *et al.*, 2023; Faloye *et al.*, 2022).

The key biochar properties that alter the shape, size, and continuity of pores and soil hydraulic properties/conductivity are large specific surface area (Lei and Zhang, 2013; Liu *et al.*, 2017; Tomczyk *et al.*, 2020), high pore volume, and particle size (Edeh *et al.*, 2020). Biochar addition to soils can also promote aggregation and stability (Feizi *et al.*, 2019; Chen *et al.*, 2022; Li *et al.*, 2023), reduce thermal conductivity, thermal diffusivity, albedo (Usowicz *et al.*, 2016), evaporation, and cracking (Zhang *et al.*, 2020), sequester carbon (Juriga and Šimanský, 2018), enhance ion absorption and exchange capacity (Gong *et al.*, 2019), alter soil hydrophobicity (Chen *et al.*, 2022; Edeh and Mašek,

*Corresponding author e-mail: j.lipiec@ipan.lublin.pl

**The work was partially funded by the HORIZON 2020, European Commission, Programme: H2020-SFS-2015-2: SoilCare for profitable and sustainable crop production in Europe, project No. 677407 (SoilCare, 2016-2021).

2022), improve aeration and microbial activity (Zhang *et al.* 2012; Fišarová *et al.*, 2024), reduce greenhouse gas emission (Li *et al.*, 2024), and enable food security by augmenting soil fertility and quality (Głąb *et al.*, 2016; Gao and DeLuca, 2022; Kumar *et al.*, 2023). A new survey indicates that carbon dioxide removal by biochar results in circular climate change mitigation and adaptation (Global Biochar Market Report, 2023). Because of the beneficial effects, the application of biochar to soils has been broadly promoted in recent decades (Lehmann, 2007; Hyväluoma *et al.*, 2018; Tomczyk *et al.*, 2020; Kumar *et al.*, 2022; Usowicz *et al.*, 2020; Fornes *et al.*, 2024). The wide biochar use was facilitated by the growth of industrial biochar production with a global production of 350 000 metric tons annually and a compound annual growth rate of 91% between 2021 and 2023 (Global Biochar Market Report 2023).

The results regarding biochar's effects on hydraulic conductivity are not consistent and scarce. Several studies on biochar-amended soils did not expose a distinctive trend concerning the increase or decrease in hydraulic conductivity values (Novak *et al.*, 2016; Usowicz and Lipiec, 2020; Chen *et al.*, 2022; Yan *et al.*, 2021; Wang *et al.*, 2022; Garg *et al.*, 2023; O'Keeffe *et al.*, 2023). Inconsistent results are largely attributed to the different biochar properties related to the type of feedstock and pyrolysis temperatures, application method, soil type, and soil water status (Ajayi *et al.*, 2016; Edeh *et al.*, 2020; Chen *et al.*, 2022; Garg *et al.*, 2023). Some studies suggest that the reduced hydraulic conductivity in biochar-amended soil is attributed to pore filling by biochar, which increases tortuosity and reduces pore throat size (Faloye *et al.*, 2022, 2024) although the soil structure is improved (Villagra-Mendoza and Horn, 2018 a,b). The scarcity of the data is related to the fact that direct measurements of the hydraulic conductivity for large areas are expensive and time-consuming. Also, the measurements often include different soil water content ranges and are valid to only a narrow range of soil saturation with water (Arya *et al.*, 1999, Nemes *et al.*, 2001). Therefore, there is a need for alternative methods for the prediction of the hydraulic conductivity in a wider range of soil water content from the more easily measured soil water retention curve (Mualem, 1976; van Genuchten and Pachepsky, 2011). The precise prediction of the soil hydraulic properties as a function of soil water status is critical for satisfactory characterization of water and nutrient movement and uptake by plants (Faloye *et al.*, 2022; Krzyszczak *et al.*, 2024). Among various predictive methods of hydraulic conductivity, based on statistical analyses of pore-size distribution, the Darcy and Poiseuille equations and regression models are widely used. Using different model approaches and/or input data from biochar experiments limits an unbiased comparison of hydraulic conductivity from other studies (Lim *et al.*, 2015).

Therefore, to minimize the secondary effects, we propose in this study to (1) evaluate the effect of the same biochar types applied to sandy soil (Zhang *et al.*, 2019) and loamy soil (Lei and Zhang, 2013) on hydraulic conductivity over a wide matric potential range assessed by the same statistical-physical model of soil conductivity (Usowicz *et al.*, 2006b) and (2) improve the modeling performance of hydraulic conductivity in biochar-amended soils by calculating the volume of variously sized capillaries and capillary length.

2. MATERIALS AND METHODS

2.1. Statistical-physical model and input data

The effect of biochar application on soil hydraulic conductivity was evaluated using the statistical-physical model of soil conductivity proposed by Usowicz *et al.* (2006b). The model is based upon the usage of the terms hydraulic resistance, capacitors (Ohm's law and Darcy's law), two Kirchhoff's laws, and multinomial distribution. Soil and biochar particles of different shapes and sizes and pores (Fig. 1a) between them are represented by a net of more or less cylindrically interconnected channels with different equivalent capillary radii (Fig. 1b'). The junction points in Fig. 1b' in the form of spheres connect the capillaries horizontally and vertically. The junction points in Fig. 1b' in the form of spheres connect the capillaries horizontally and vertically. When such a porous medium is considered, a statistical approach for the description of the liquid or gas flow can be applied. The soil and biochar phases and their configuration are decisive for the pore distribution and the course of the water retention curve in this medium. The statistical-physical model considers the pore space as the capillary net that is represented by parallel and serial connections of hydraulic resistors in the layer and-between the

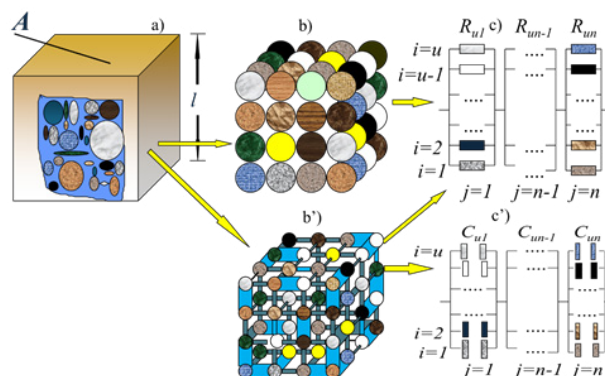


Fig. 1. Schematic diagram of the statistical-physical model construction, a) soil unit volume, b) a system of spheres considered as soil particles forming overlapping layers, b') a system of air and water capillaries between soil particles forming overlapping layers, c) a system parallel connection of thermal, electrical and hydraulic resistors in the layers and series between layers, c') a system parallel connection of heat, electrical and hydraulic capacitors in the layers and series between the layers.

layers, respectively. A system of spheres forming overlapping layers in Fig. 1b represents thermal resistors, electrical resistors, and electrical capacitors.

The hydraulic conductivity of a porous medium is expressed by the mean hydrodynamic radius of the Hagen-Poiseuille's equation, K :

$$K = \frac{\rho g}{8\eta} r^2, \quad (1)$$

like the hydraulic conductivity of an elemental capillary in the net K_{ij} :

$$K_{ij} = \frac{\rho g}{8\eta} r_{ij}^2, \quad (2)$$

where: r denotes a capillary radius, ρ – liquid density, g – acceleration of gravity, η is liquid viscosity. Inserting K and K_{ij} into the equation for the total resistance of a parallel and serial configuration of resistors:

$$R = \sum_{j=1}^n R_j = \sum_{j=1}^n \frac{1}{\sum_{i=1}^u \frac{1}{R_{ij}}}, \quad (3)$$

where:

$$R = \frac{l}{KA} \quad \text{and} \quad R_{ij} = \frac{l_{ij}}{K_{ij}A_{ij}}, \quad (4)$$

and assuming that A corresponds to u mean surface areas πr^2 , A_{ij} equals πr_{ij}^2 , and there are n unit serial connections in the length l :

$$\frac{l}{AK} = \sum_{j=1}^n \frac{1}{\sum_{i=1}^u \frac{1}{\frac{l_{ij}}{K_{ij}A_{ij}}}}, \quad (5)$$

after substituting, we arrive at an equation for the calculation of a mean hydrodynamic squared radius:

$$r^2 = \sqrt{\frac{1}{\frac{u}{n} \sum_{j=1}^n \frac{1}{\sum_{i=1}^u \frac{r_{ij}^4}{l_{ij}}}}}. \quad (6)$$

Putting r^2 again into the equation for K calculation with a mean hydrodynamic radius:

$$K = \frac{\rho g}{8\eta} \sqrt{\frac{1}{\frac{u}{n} \sum_{j=1}^n \frac{1}{\sum_{i=1}^u \frac{r_{ij}^4}{l_{ij}}}}}, \quad (7)$$

and following the method applied earlier for the model of electric conductivity, we can set down a general equation for hydraulic conductivity (Usowicz, 2000):

$$K = \frac{\rho g}{8\eta} \sqrt{\frac{1}{u \sum_{j=1}^L \frac{P(x_1 f_1 \dots x_k f_k)}{x_1 l_1 + \dots + x_k l_k}}}, \quad (8)$$

where: L is the number of all possible combinations of the capillary configuration, x_1, x_2, \dots, x_k – number of capillaries formed between the particles of the medium with a capillary radius of r_1, r_2, \dots, r_k , and length l_1, l_2, \dots, l_k , u – number of the degrees of freedom (number of parallel connections of resistors), where $\sum_{i=1}^k x_{ij} = u$, $j=1, 2, \dots, L$. $P(x_{ij})$ is the

probability of occurrence of a given capillary configuration calculated from the multinomial distribution (Eadie *et al.*, 1971):

$$P(x_1, x_2, x_3, x_4, x_5, x_6) = \frac{u!}{x_1! x_2! x_3! x_4! x_5! x_6!} f_1^{x_1} f_2^{x_2} f_3^{x_3} f_4^{x_4} f_5^{x_5} f_6^{x_6}, \quad (9)$$

$P(x_{ij})$ – describes the probability of the event that in u independent trials exactly x_{ij} results of the j type were obtained, if the probability of i results in a single trial is f_i , $i = 1, 2, \dots, k$. The condition: $\sum_{j=1}^L P(C=x_j) = 1$ must also be fulfilled.

Capillary size radii and the probability of occurrence of a given capillary configuration were calculated based on the measured water retention curve (Fig. 2) and saturated water content. It was assumed that the water retention curves are divided into k parts (in our case into five parts), which are not necessarily equal, but may also be equal.

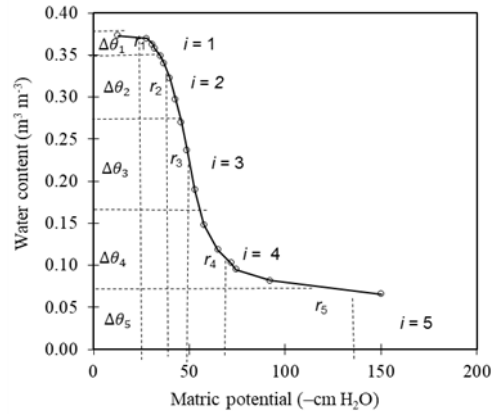


Fig. 2. Determination of the mean capillary radius (r_i) and volumetric water content ($\Delta\theta_i$), $i = 1, 2, \dots, 5$, from the water retention curve. The data used in this example are taken from Brooks and Corey (1964).

The probability of selecting a specific capillary in a single sample was calculated from equations: $f_1 = \Delta\theta_1/\phi$, $f_2 = \Delta\theta_2/\phi$, $f_3 = \Delta\theta_3/\phi$, $f_4 = \Delta\theta_4/\phi$, $f_5 = \Delta\theta_5/\phi$, and $f_6 = (\phi - \theta)/\phi$, where $\Delta\theta_i$ are water contents at individual suction points determined from the retention curve, θ current soil water content, ϕ porosity, and $\phi - \theta$ air content.

The input data from field experiments conducted on sandy and loamy soils in China were used in this study. The experimental field on sandy soil (97.8% sand and 2.2% silty sand) containing 0.581% of organic carbon was located in the Desert Ecosystem Research Station in the transitional zone of Minqin County, Gansu province (38° 34'N, 102° 58' E) (Zhang *et al.*, 2019). The seven treatments were as follows: soil only serving as the control (CK); soil with woodchip biochars pyrolyzed at 300°C (SWL) and 700°C (SWH); soil with rice straw biochars pyrolyzed at 300°C (SRL) and 700°C (SRH); and soil with dairy manure biochars pyrolyzed at 300°C (SDL) and 700°C (SDH). Each of the six biochars was mixed at a mass ratio of 5% (w/w) with the soil (0-15 cm depth) with three replications per

treatment, and the mixtures were incubated at 25°C for 180 days. The soil water retention curve was determined with a high-speed refrigerated centrifuge (Hitachi's SCR22G, Japan) using a glass cylinder with 30 mm of height and 45 mm of diameter filled with pure soil or soil-biochar mixtures at soil water content < 10% of the saturated water content. Briefly, a sample was saturated with gas-free water for 48 h and weighed for initial mass and saturated water content. The saturated soil samples were centrifuged at rotation speeds of 500, 900, 1 500, 2 500, 3 500, 4 500, 5 500, and 6 500 rpm for 60 min, and at 7 500 rpm for 100 min, respectively. The soil water suction h is related to rotation speeds (Feng *et al.*, 2009).

The experimental field on loamy soil (40% sand, 35% silt, and 25% clay) containing 1.07% of organic carbon was located in the Dinghushan Nature Reserve (23°09'21"–23°11'30"N, 112°30'39"–112°33'41"E, 100–700 mH), Guangdong Province (Lei and Zhang, 2013). The treatments included soil only used as the control (CK); SDL (soil+dairy manure pyrolyzed at 300°C), SDM (soil+dairy manure pyrolyzed at 500°C), SDH (soil+dairy manure pyrolyzed at 700°C), SWL (soil+woodchip pyrolyzed at 300°C), SWM (soil+woodchip pyrolyzed at 500°C), and SWH (soil+woodchip pyrolyzed at 700°C). Each of the six biochars was mixed at a mass ratio of 5% (w/w) with the soil (0–10 cm depth) with three replications per treatment and the mixtures were incubated at 25°C for 180 days. The soil water retention curve was determined with the hanging water column and pressure plate methods (Klute, 1986) using a glass cylinder with 30 mm of height and 45 mm of diameter filled with pure soil or soil-biochar mixtures at a soil water content of 80% of the field capacity.

The values of hydraulic conductivity and water contents in the biochar-amended soils (soil + biochar mixtures) for different matric potential values (–cm of H₂O) in the range of 0 to –15 000 for the statistical-physical model of hydraulic conductivity were calculated from the van Genuchten

equation (van Genuchten, 1980). The equivalent capillary radii were computed using the Young-Laplace equation: $r_i = 1491.3/h$ (h = heights of the H₂O column in –cm). This matric potential range was divided into five sub-regions of the water column h : from 0 to –40 cm, from –40 to –100 cm, from –100 to –200 cm, from –200 to –1 500, and from –1 500 to –15 000 cm H₂O (Fig. 3a,b). For each of them, the average capillary radii (360.4, 23.3, 11.5, 3.6, 0.53, and 0.24 μ m) and the corresponding volumes of water content were calculated. The 6th capillary conducting water through water vapor and liquid water films on soil and biochar particles in the model was estimated/assumed to have a 0.24 μ m radius, corresponding to the matric potential around –5020 cm H₂O at which plants suffer stress due to water shortage. With soil water loss, the first 5 capillaries with 360.4 to 0.53 μ m radii will dewater one by one. On the other hand, the air content will increase in the 6th capillary, which means an increase in the probability of flow through water vapor and water films. This capillary may have a constant radius assumed for a specific matric potential or estimated from experimental data, *e.g.*, at residual water content, or from known physical relationships that are responsible for water flows through vapor partly through water films on solid soil particles. Below this water content, the 6th capillary radius will change exponentially: $r_6(\theta) = ae^{b\theta}$ with the change in soil water content – θ , where a and b are the parameters of the equation. The value of the radius of the 6th capillary at the so-called residual/reference water content will decrease as a function of soil water content.

Using the saturated hydraulic conductivities and the water retention curve, the equivalent capillary lengths and degrees of freedom u (the number of parallel connections of resistors) for different media and soils were selected by comparing the calculated and measured results and the best agreement between the results (Usowicz, 2000). The model was validated against measured water retention and

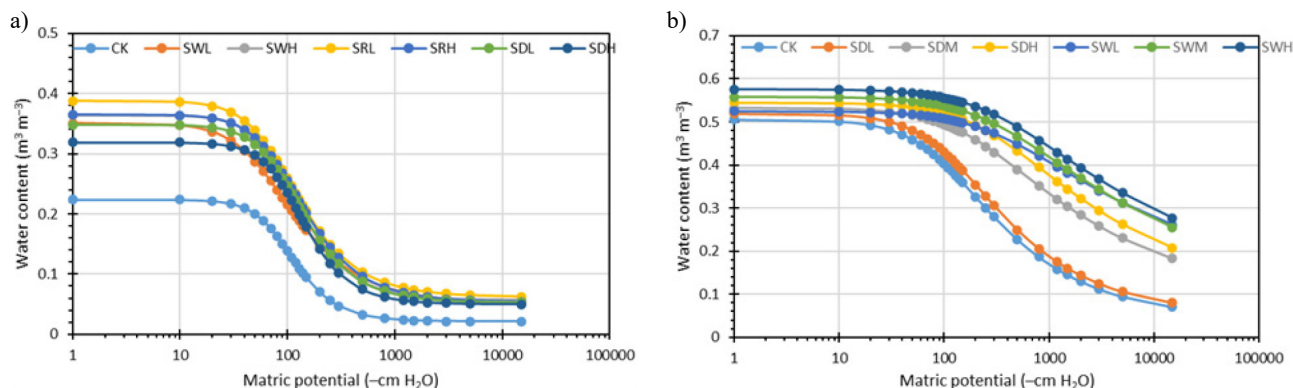


Fig. 3. Water retention curves of sandy soil (a) and loamy soil (b). Control without biochar (CK), woodchip biochar pyrolyzed at 300°C (SWL), woodchip biochar pyrolyzed at 700°C (SWH), rice straw biochar pyrolyzed at 300°C (SRL), rice straw biochar pyrolyzed at 700°C (SRH), dairy manure biochar pyrolyzed at 300°C (SDL), dairy manure biochar pyrolyzed at 700°C (SDH), dairy manure pyrolyzed at 500°C (SDM), woodchip biochar pyrolyzed at 500°C (SWM). Based on data from Zhang *et al.* (2019) for the sandy soil and from Lei and Zhang (2013) for the loamy soil.

water conductivity curves in the saturated and unsaturated zones for Lakeland sand soil and Hygiene and Berea rocks (Usowicz, 2000, 2001).

2.2. Statistical evaluation

Differences in the water content (WC) and calculated hydraulic conductivity (HC) between the biochar amended and control plots (CK) were evaluated based on the root mean square residuals (*RMSR*) and maximum relative residuals (*MRR*). The *RMSR* and *MRR* were calculated as:

$$RMSR = \sqrt{\frac{\sum_{i=1}^n (f_{mi} - f_{ci})^2}{k}}, \quad (10)$$

$$MRR = \max_{i=1,2,\dots,n} \left\{ \left| \frac{f_{mi} - f_{ci}}{f_{mi}} \right| 100\% \right\}, \quad (11)$$

where: f_{mi} is the control plot data, f_{ci} is the biochar-amended plot data, $k = n - 1$ if $n < 30$, and $k = n$ if $n > 30$. In our study $n = 27$ data points for both water retention curve and hydraulic conductivity curve at the following matric potentials (in $-\text{cm H}_2\text{O}$): 1, 10, 20, 30, 40, 50, 60, 70, 80, 90, 100, 110, 120, 130, 140, 150, 200, 250, 300, 500, 800, 1200,

1500, 2000, 3000, 5000 and 15000. The results of the equations were presented as averages over the three replicates for each biochar type in each soil type.

3. RESULTS

3.1. Soil properties and parameters of the statistical-physical model

As can be seen from Table 1, pH, organic carbon content C (in %), and SSA (in $\text{m}^2 \text{g}^{-1}$) were 8.72, 0.581, and 3.36 in control sand and 4.25, 1.07, and 11.5 in loam soils. The ranges of the properties in biochars added to the sand and loam soil were 7.95-11.2, 37.8-66.4%, 1.4-392 $\text{m}^2 \text{g}^{-1}$ and 7.46-10.1, 19-51.2%, 14.3-124 $\text{m}^2 \text{g}^{-1}$, respectively.

We assumed in this work that the best agreement between the calculated and measured results of capillary lengths would occur using 7 degrees of freedom. The equivalent capillary lengths l (m) calculated with the statistical-physical model in the sandy soil were similar in the control and treatments with woodchip biochar pyrolyzed at 300°C (SWL) and rice straw biochars pyrolyzed at 300°C (SRL) (1.12-1.17); they appreciably decreased (to 0.42-0.597)

Table 1. Parameters of the statistical-physical model: degree of freedom ($u=7$), equivalent capillary length (l), bulk density (BD), saturated hydraulic conductivity (Ksat), and physicochemical properties of the studied soils

Sandy soil								
Properties*	Unit	CK	SWL	SWH	SRL	SRH	SDL	SDH
Capillary length	l (m)	1.13	1.12	0.597	1.17	0.64	0.43	0.42
Bulk density ¹	Mg m^{-3}	1.53	1.17	1.24	1.2	1.25	1.23	1.27
pH ⁽¹⁾	Unitless	8.72	7.95	10.6	9.24	12	8.68	11.2
C ⁽¹⁾	(%)	0.581	66.4	85.7	57	59.9	40.4	37.8
SSA ⁽¹⁾	($\text{m}^2 \text{g}^{-1}$)	3.36	1.4	392	2.11	187	3.59	168
Measured Ksat ¹	(m s^{-1})	6.135×10^{-5}	5.215×10^{-5}	5.522×10^{-5}	3.823×10^{-5}	3.540×10^{-5}	4.602×10^{-5}	4.554×10^{-5}
Calculated Ksat	(m s^{-1})	6.138×10^{-5}	5.216×10^{-5}	5.222×10^{-5}	3.824×10^{-5}	3.536×10^{-5}	4.618×10^{-5}	4.567×10^{-5}
Loamy soil								
Properties	Unit	CK	SDL	SDM	SDH	SWL	SWM	SWH
Capillary length	l (m)	3.2	2.3	13	20	72	36	45
Bulk density ²	(Mg m^{-3})	1.190	1.071	1.052	1.062	1.010	1.049	1.051
pH ⁽²⁾	Unitless	4.25±0.03	7.46±0.01	9.28±0.09	9.70±0.03	7.16±0.04	7.96±0.04	10.1±0.12
C ⁽²⁾	(%)	1.07	39.3	19	27.9	51.2	43.2	31.1
SSA ⁽²⁾	($\text{m}^2 \text{g}^{-1}$)	11.5	14.3	44.1	83.4	24.04	67.3	124
Measured Ksat ²	(m s^{-1})	6.898×10^{-6}	7.037×10^{-6}	7.153×10^{-6}	6.968×10^{-6}	9.005×10^{-6}	9.838×10^{-6}	1.028×10^{-5}
Calculated Ksat	(m s^{-1})	6.868×10^{-6}	7.011×10^{-6}	7.154×10^{-6}	6.989×10^{-6}	9.057×10^{-6}	9.837×10^{-6}	1.033×10^{-5}

*Based on data from: ¹Zhang *et al.* (2019), ²Lei and Zhang (2013). Control without biochar (CK), woodchip biochar pyrolyzed at 300°C (SWL), woodchip biochar pyrolyzed at 700°C (SWH), rice straw biochar pyrolyzed at 300°C (SRL), rice straw biochar pyrolyzed at 700°C (SRH), dairy manure biochar pyrolyzed at 300°C (SDL), dairy manure biochar pyrolyzed at 700°C (SDH), dairy manure pyrolyzed at 500°C (SDM), woodchip biochar pyrolyzed at 500°C (SWM), BD – bulk density measured by the core method, pH – measured using pH probe with a suspension in H_2O ; C – organic carbon measured using commercial analyzer, SSA – the specific surface area measured with N2-BET method in¹ and Brunauer, Emmett, and Teller nitrogen adsorption technique in². The standard deviations in the sandy soil for the measured Ksat varied from 2.77×10^{-8} (at SRH) to 5.55×10^{-7} (at SWL). Corresponding values for the loamy soil were 6.94×10^{-7} (at SDM) and 2.22×10^{-6} (at SWL).

under the remaining treatments. Regarding the loamy soil, the equivalent capillary length under control and SDL are similar (2.3–3.2 m) and appreciably increased under the remaining biochar treatments (13–72 m). According to the model assumptions, the higher equivalent capillary lengths may indicate higher capillary tortuosity. The bulk density in both soils was lower in the biochar-amended than in the control plots, especially in the sandy soil. Irrespective of soil texture, the variability of bulk density was low, as shown by the relatively low standard deviations (the maximum of 0.04 Mg m^{-3}).

3.2. Soil water retention, hydraulic conductivity, and capillary properties

As can be seen, from Fig. 3a, adding all biochar types into the sandy soil resulted in higher soil water contents at the whole matric potential range from saturation ($-1 \text{ cm H}_2\text{O}$) to wilting point ($-15\,000 \text{ cm}$). The effect was most pronounced in the treatment including soil + rice straw biochar pyrolyzed at 300°C (SRL), where the soil water content increased by around 70–200%, depending on the matric potential, compared to the control (CK). Irrespective of the matric potential, the differences in the soil water content were appreciably lower between the biochar types than between the control soil (CK) and each biochar type. The soil water content at field water capacity (at matric potential -100 cm) being $0.13 \text{ m}^3 \text{ m}^{-3}$ in CK increased in all the biochar treatments by around 61 to 108% ($\sim 0.21\text{--}0.27$ vs. $\sim 0.13 \text{ m}^3 \text{ m}^{-3}$, depending on the biochar type).

Also, adding biochars in the loamy soil (Fig. 3b) increased soil water content in the whole matric potential range. The highest and lowest increase was recorded under the treatments with soil+woodchip pyrolyzed at 700°C (SWH) and soil+dairy manure pyrolyzed at 300°C (SDL), respectively. Depending on the matric potential, the increase ranged from around 14 to 290% in the former and from 2.6 to 13% in the latter. The soil water content at field

water capacity was $\sim 0.40 \text{ m}^3 \text{ m}^{-3}$ in CK and increased in most biochar treatments by 22 to 45.0% except SDL, which was close to that in the control ($0.42 \text{ m}^3 \text{ m}^{-3}$). As expected, the soil water content at comparable matric potentials and treatments was greater in the loamy than sandy soil (Fig. 3a,b).

The effect of the biochars on the hydraulic conductivity was related to the potential and soil type (Fig. 4a,b). In the sandy soil, the hydraulic conductivity at the wet range of matric potential from -1 to around $-10 \text{ cm H}_2\text{O}$ under SWL and from 1 to around $-70 \text{ cm H}_2\text{O}$ under the remaining biochar treatments was lower by 9 to 25%, at the drier range (from around -500 to $-15\,000 \text{ cm H}_2\text{O}$) it was higher by 1.6 to 19% (Fig. 4a). The addition of all biochar types into the loamy soil increased hydraulic conductivity, compared to the control across the whole matric potential range (Fig. 4b). The highest and similar increase was observed under SWL (soil+woodchip pyrolyzed at 300°C), SWM (soil+woodchip pyrolyzed at 500°C), and SWH (soil+woodchip pyrolyzed at 700°C). The lowest increase was recorded under SDL (soil + dairy manure pyrolyzed at 300°C). The greatest increases were noted at the matric potential from -100 to around $-5000 \text{ cm H}_2\text{O}$. At the characteristic matric potential ($-100 \text{ cm H}_2\text{O}$) corresponding to field water capacity (FC), the hydraulic conductivities under all biochar treatments in the sandy soil were slightly higher (to around 8%) than in the control ($1.00 \times 10^{-6} \text{ m s}^{-1}$), while in the loamy soil they increased from around 5% in the treatments with dairy manure pyrolyzed at 300°C (SDL) biochar to 50–80% in the remaining biochar variant.

In the sandy soil, the *RMSR* values for WC varied between 0.079 and $0.114 \text{ m}^3 \text{ m}^{-3}$ and the lowest values were in SDH, SWL ($0.079\text{--}0.080 \text{ m}^3 \text{ m}^{-3}$), and the largest in SRL, and SRH ($0.104\text{--}0.114 \text{ m}^3 \text{ m}^{-3}$) (Table 2). In treatments with biochars derived from woodchip (SW), the *RMSR* values increased with increasing pyrolysis temperature (from 0.08 to $0.10 \text{ m}^3 \text{ m}^{-3}$) and decreased in plots with biochars derived from rice straw (SR) (from 0.114 to $0.104 \text{ m}^3 \text{ m}^{-3}$).

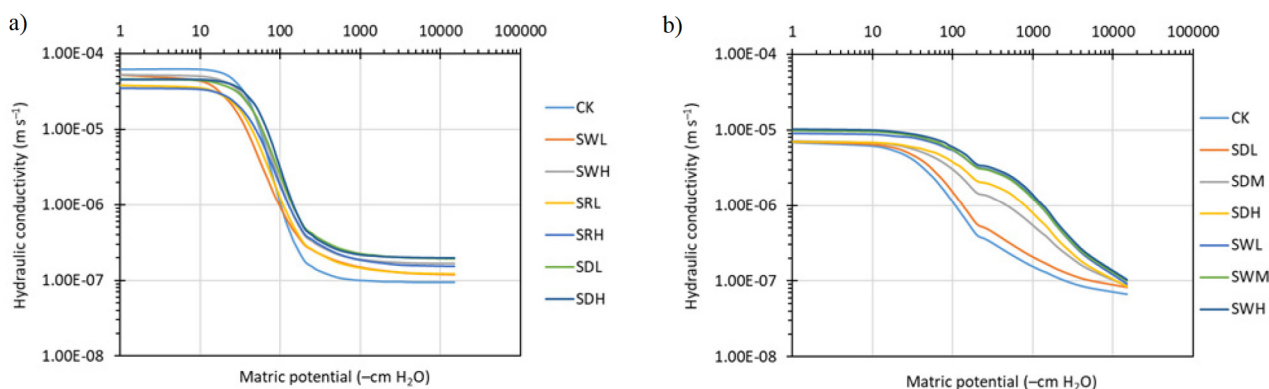


Fig. 4. Calculated soil hydraulic conductivity as a function of the matric potential from the statistical-physical model of sandy soil (a) and loamy soil (b). Input data from Zhang *et al.* (2019) for the sandy soil and Lei and Zhang (2013) for the loamy soil. Control without biochar (CK), woodchip biochar pyrolyzed at 300°C (SWL), woodchip biochar pyrolyzed at 700°C (SWH), rice straw biochar pyrolyzed at 300°C (SRL), rice straw biochar pyrolyzed at 700°C (SRH), dairy manure biochar pyrolyzed at 300°C (SDL), dairy manure biochar pyrolyzed at 700°C (SDH), dairy manure pyrolyzed at 500°C (SDM), woodchip biochar pyrolyzed at 500°C (SWM).

and dairy manure (SD) (from 0.094 to 0.079 m³ m⁻³). The lowest *RMSR* values for HC were found in treatments with biochars derived from SWH (3.81×10^{-6} m s⁻¹) and largest in treatments with biochars derived from SWL, SRL, and SRH (between 8.77 and 9.80×10^{-6} m s⁻¹) without a clear effect of pyrolysis temperature. The *RMSR* values for the WC and HC at comparable temperatures were lowest in plots with SW biochars and highest in SR biochars. The *MRR* values for WC decreased with increasing pyrolysis temperature and increased for HC, irrespective of the biochar type added. The highest *MRR* was recorded for SRL (234.6%) and the lowest for SDL (176.9%), while at high pyrolysis temperature, it was highest for SRH (200%) and lowest for SDH (142.9%). As to HC, the *MRR* was higher in SDL (179.4%) than in SWL and SRL (69.7-70.6%) and SDH (211.4%) than in SWH and SRH (118.7-132%).

As can be seen from Fig. 5a, the addition of all biochars to the sandy soil increased the volume of all capillaries by 14% (from 0.071 m³ m⁻³ to 0.081 m³ m⁻³) for capillary 23.3 µm under the dairy manure biochars pyrolyzed at 300°C (SDL) up to 228% (from 0.014 to 0.046 m³ m⁻³) for capillary 360.4 µm under the woodchip biochars pyrolyzed at 300°C (SWL). The volumes of capillaries with 360.4 and 23.3 µm radii in the soil enriched with dairy manure biochar pyrolyzed at 700°C and 11.5 µm in the treatment with woodchip biochars pyrolyzed at 300°C (SWL) remained unchanged. Consequently, the volume of the capillary with a 0.24 µm radius that conducts water through vapor water films in the model increased in all biochar treatments by around 42% in SDH to 73% in SRL, compared to the control (0.224 m³ m⁻³).

The standard deviations (SD) of water content for capillaries with radii of 360.4 and 23.3 µm in the sandy soil were the smallest, from 0.0007 to 0.0057 m³ m⁻³ and for the remaining capillaries from 0.0058 to 0.0269 m³ m⁻³. In the case of the capillary with a radius of 0.53 µm, the SD value was 2.4-2.9 times higher in the biochar treatments than in the control CK (0.09 m³ m⁻³) (Fig. 5a).

As to the loamy soil (Fig. 5b), the contents of water retained in larger capillaries (from 360.4 to 3.6 µm radius) decreased in all the biochar-amended plots except in that amended with dairy manure biochar pyrolyzed at 300°C (SDL), where the contents were slightly larger or slightly smaller compared to the control. The high relative reduction (83-84%) was observed for capillary radii 360.4 and 23.3 µm in all the remaining biochar treatments, compared to the control values (0.035 and 0.067 m³ m⁻³, respectively). However, the contents of water retained in smaller capillaries with the 0.53 µm radius being 0.145 m³ m⁻³ increased in all the biochar-amended plots by 10 to 185%, depending on the biochar type. Also, the volume of capillaries with the 0.24 µm radius in control (0.506 m³ m⁻³) increased in all the biochar treatments in the 2.6-14% range. The lowest and largest increases in the content of capillaries with the 0.53 and 0.24 µm radii were observed in variants with additions of dairy manure biochar pyrolyzed at 300°C (SDL) and woodchip biochar pyrolyzed at 700°C (SWH), respectively.

The SD of water content for capillaries with radii of 360.4, 23.3, and 11.5 µm in the loamy soil were the smallest from close to 0 to 0.01 m³ m⁻³, and for the remaining capillaries from 0.01 to 0.11 m³ m⁻³. In the case of the capillary

Table 2. Root mean square residuals (*RMSR*) and maximum relative residuals (*MRR*) of differences in the water content and calculated hydraulic conductivity between the biochar-amended and control plots (CK)

Sandy soil* ¹	Property	<i>RMSR</i>	<i>MRR</i> (%)	Loamy soil ²	<i>RMSR</i>	<i>MRR</i> (%)
SWL	WC (m ³ m ⁻³)	0.08	203.8	SDL	0.022	12.7
	HC (m s ⁻¹)	8.77×10^{-6}	69.7		3.55×10^{-7}	41.0
SWH	WC (m ³ m ⁻³)	0.1	181.8	SDM	0.114	157.7
	HC (m s ⁻¹)	3.81×10^{-6}	118.7		1.36×10^{-6}	311.1
SRL	WC (m ³ m ⁻³)	0.114	234.6	SDH	0.144	191.5
	HC (m s ⁻¹)	9.78×10^{-6}	70.6		1.90×10^{-6}	532.3
SRH	WC (m ³ m ⁻³)	0.104	200	SWL	0.156	267.6
	HC (m s ⁻¹)	9.80×10^{-6}	132		3.23×10^{-6}	910.3
SDL	WC (m ³ m ⁻³)	0.094	176.9	SWM	0.172	259.2
	HC (m s ⁻¹)	5.77×10^{-6}	179.4		3.44×10^{-6}	878.6
SDH	WC (m ³ m ⁻³)	0.079	142.9	SWH	0.192	290.1
	HC (m s ⁻¹)	5.46×10^{-6}	211.4		3.88×10^{-6}	998.0

*Based on measurement data from: ¹Zhang *et al.* (2019) and ²Lei and Zhang (2013). Woodchip biochar pyrolyzed at 300°C (SWL), woodchip biochar pyrolyzed at 700°C (SWH), rice straw biochar pyrolyzed at 300°C (SRL), rice straw biochar pyrolyzed at 700°C (SRH), dairy manure biochar pyrolyzed at 300°C (SDL), dairy manure biochar pyrolyzed at 700°C (SDH), dairy manure pyrolyzed at 500°C (SDM), woodchip biochar pyrolyzed at 500°C (SWM).

with a radius of $0.53\ \mu\text{m}$ similar SD values in CK and SDL ($0.024\text{--}0.027$) were from 2.9 to 4.7 times higher in the remaining treatments (Fig. 5b).

In the loamy soil, the *RMSR* values for WC varied between 0.022 in SDL and $0.192\ \text{m}^3\ \text{m}^{-3}$ in SWH and for HC between 3.55×10^{-7} in SDL and $3.88 \times 10^{-6}\ \text{m}\ \text{s}^{-1}$ in SWH and increased with pyrolysis temperature irrespective of biochar substrate (Table 2). The *MRR* values for WC varied between 12.7 and 290.1% and between 41 and 998% for HC. The values of both metrics were lowest in SDL, intermediate for SDM and SDH, and highest for SWL, SWM, and SWH. The *MRR* values for WC increased with pyrolysis temperature in SD biochars (from 12.7 to 191.5%) while in SW biochars it was relatively high for all temperatures (259.2–290.1%). For HC it increased with pyrolysis temperature in SD biochars (41.0 to 523.3%) and was very high in SW biochars at all pyrolysis temperatures (878.6 to 998.0%). The *RMSR* and *MRR* values were higher

in SD than in SW at all comparable temperatures. Both the *RMSR* and *MRR* ranges were larger in loamy than in sandy soil (Table 2).

3.3. Probability of occurrence of a given capillary configuration

The effect of the biochars on the probability of occurrence of a given capillary (fraction of the sixth capillary with the $0.24\ \mu\text{m}$ radius) was related to soil type (Fig. 6a,b). In sandy soil, the probability of capillary $360.4\ \mu\text{m}$ being 0.062 in control increased to 0.132 after the addition of woodchip biochar pyrolyzed at 300°C (SWL) and under the remaining biochar treatments it increased or decreased within the range from 0.04 to 0.086 (Fig. 6a). As to the capillaries 23.3 and $11.5\ \mu\text{m}$ the probabilities of occurrence being respectively 0.317 and 0.308 in control decreased in all biochar treatments to 0.223–0.252 and 0.194–0.294, respectively. The probability of occurrence in capillaries

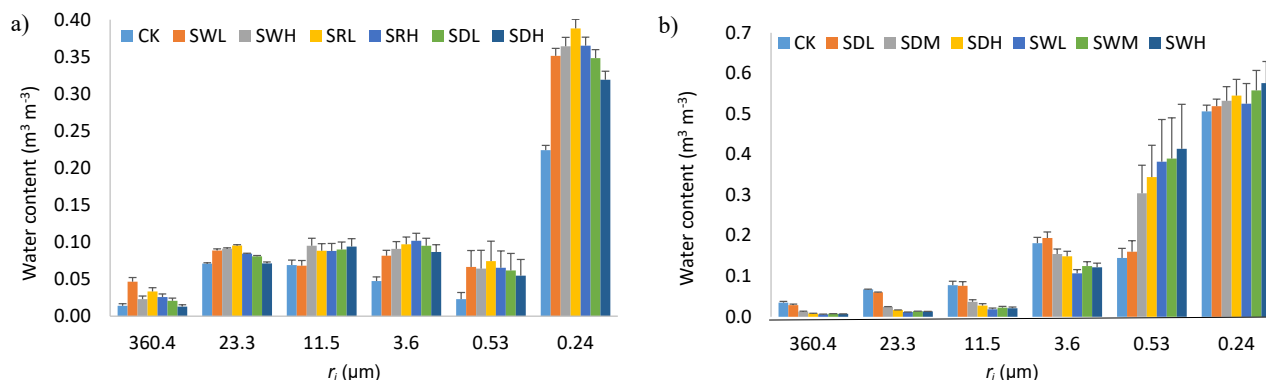


Fig. 5. Calculated water content in soil capillaries with different radii from the statistical-physical model for sandy soil (a) and loamy soil (b). Control without biochar (CK), woodchip biochar pyrolyzed at 300°C (SWL), woodchip biochar pyrolyzed at 700°C (SWH), rice straw biochar pyrolyzed at 300°C (SRL), rice straw biochar pyrolyzed at 700°C (SRH), dairy manure biochar pyrolyzed at 300°C (SDL), dairy manure biochar pyrolyzed at 700°C (SDH), dairy manure pyrolyzed at 500°C (SDM), woodchip biochar pyrolyzed at 500°C (SWM). Bars represent standard deviation ($n = 5\text{--}7$ for 5 capillaries with radii between 360.4 and $0.53\ \mu\text{m}$ and 31 for capillaries with a radius of $0.24\ \mu\text{m}$).

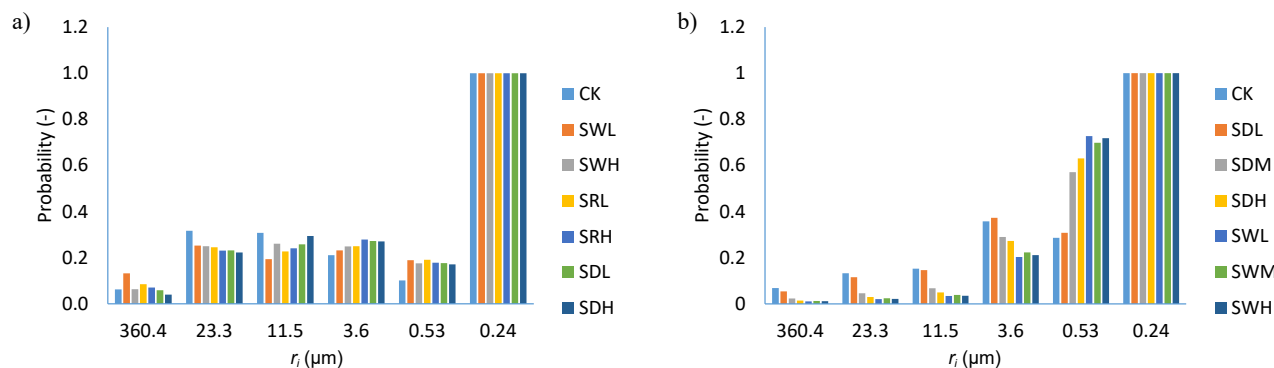


Fig. 6. Calculated probability of the occurrence of soil capillaries with different radii (r_i) from the statistical-physical model for sandy soil (a) and loamy soil (b). Control without biochar (CK), woodchip biochar pyrolyzed at 300°C (SWL), woodchip biochar pyrolyzed at 700°C (SWH), rice straw biochar pyrolyzed at 300°C (SRL), rice straw biochar pyrolyzed at 700°C (SRH), dairy manure biochar pyrolyzed at 300°C (SDL), dairy manure biochar pyrolyzed at 700°C (SDH), dairy manure pyrolyzed at 500°C (SDM), woodchip biochar pyrolyzed at 500°C (SWM).

with the 3.64 and 0.53 μm radii in control (0.211 and 0.102, respectively) increased after adding all biochars to 0.223-0.252 and 0.171-0.191, respectively. Irrespective of the capillary size, the probability differences were more pronounced between the control and any biochar treatments than between the biochar treatments.

In the loamy soil, the addition of all biochars decreased the probability of occurrence of larger capillaries 360.4, 23.3, 11.5, and 3.6 μm radius and increased that of capillary 0.53 μm radius (Fig. 6b). The most pronounced effect of the biochar treatments was observed with capillary 0.53 μm , where the probability of occurrence increased from 0.287 in CK to 0.728 under woodchip pyrolyzed at 300°C (SWL). Irrespective of the capillary size, the effect of the dairy manure pyrolyzed at 300°C (SDL) addition on the alterations in the probability of occurrence was much lower, than in the remaining biochars.

Irrespective of the biochar treatment, the probabilities of occurrence of the large capillaries (360.4-11.5 μm radius) were greater in the sandy soil (0.04-0.317) than in the loamy soil (0.012-0.153), while for the smaller capillary with the 0.53 μm radius, they were greater for the loamy soil (0.287-0.728) than the sandy soil (0.102-0.189). In the case of the capillary with the 3.64 μm radius, the probabilities of occurrence were similar in both soils (0.21-0.358) (Fig. 6a,b).

4. DISCUSSION

4.1. Hydraulic properties

The analysis of the results implies that the addition of biochar derived from woodchip pyrolyzed at 300°C (SWL), 500°C (SWM), and 700°C (SWH) to the loamy soil resulted in the highest volume fraction of water stored in the capillary with the 0.53 μm radius (0.382-0.414 m^3m^{-3} vs. 0.145 m^3m^{-3} in the control) (Fig. 5b) and hydraulic conductivity across the whole potential range (Fig. 4b). It is worth noticing that such a clear effect was not observed in response to the application of the remaining types of biochar to the loamy soil and all types of biochar to the sandy soil. This implies that the interactions of woodchip biochars and fine textural particles in the loamy soil contribute to an altered pore structure, connectivity, and continuity (Lei and Zhang, 2013; Faloye *et al.*, 2022) to increase hydraulic conductivity. The absence of significant differences caused by the different pyrolysis temperatures supports the dominating effect of the biochar feedstock on the formation of the pore structure and hydraulic conductivity. The data on hydraulic conductivity as a function of matric potential in the biochar-amended soils obtained in this study along with the ability of biochar to increase soil water storage capacity reported in other studies provide useful information in irrigation management and soil hydrology focused on more effective water use and soil protection in the face of the changing climate (*e.g.* Sohi *et al.*, 2009).

Our study showed that the equivalent capillary length in the control (CK) and treatment with the rice straw biochar (SRL) pyrolyzed at 300°C (1.12-1.17 m) was appreciably reduced in the remaining biochar treatments (0.42-0.597 m) but increased from 2.3-3.2 m in the loamy soil in CK and dairy manure pyrolyzed at 300°C (SDL) up to 13-72 m in the other biochar treatments. This high variation of the equivalent capillary length indicates a high capacity of the biochars to change the capillary properties but in different ways in sandy soil and loamy soil. Data on the capillary properties is a useful variable for assessing Darcy flux, soil water content and storage, capillary pressure head, and capillary rise and recirculation of water during infiltration and drainage (Kroes *et al.*, 2018; Aldrees and Nachabe, 2019).

4.2. Suitability of the statistical-physical model

Our previous works showed that the statistical-physical model is a useful tool for the prediction of the thermal conductivity of soils, depending on the mineralogical composition, water content, bulk density, temperature (Usowicz *et al.*, 2006a), soil structure (Usowicz *et al.*, 2013), biochar content (Usowicz *et al.*, 2016, 2020), electrical conductivity, and gaseous diffusivity (Usowicz, 2020). Hence, the results of this study indicate the suitability of the model to predict hydraulic conductivity, increase its performance capability, and allow the prediction of several conductivities under the same experiment. In the biochar-amended soil with the presence of macropores, the volume of the largest capillary (360.4 μm radius) considered in this study or macroporosity data from another method (*e.g.* X-ray computer tomography) can be suitable for predicting preferential flow in biochar-amended soils using the statistical-physical model.

It is important to note that the prediction of soil hydraulic conductivity can be influenced by the biochar hydrophobicity that is not considered in the statistical-physical model. Some studies have reported that biochar additions do not increase soil hydrophobicity (Kinney *et al.*, 2012; Barnes *et al.*, 2014) and increase water interception by the presence of oxygen-containing functional groups (Suliman *et al.*, 2017; Villagra-Mendoza and Horn, 2018a). In general, biochars pyrolyzed at temperatures between 400°C and 600°C support appropriate hydrological conditions and low hydrophobicity (Kinney *et al.*, 2012; Kameyama *et al.*, 2019; Edeh and Mašek, 2022). Other studies reported that some biochars can have water-repellent properties due to the occurrence of organic materials on their surface or within pores (Blanco-Canqui, 2017; Zhang *et al.*, 2019). In a study conducted by Ajayi *et al.* (2016), the repellency index increased with increasing cycles of wetting and drying and the dosage of biochar, especially in a sandy substrate. The above results imply that the performance of the statistical-physical model will depend on the amount and type of biochar added, the texture of the soil, and the pyrolysis temperature. More information on the shared

role of these factors in modifying soil hydraulic properties will further advance the performance and applicability of this model.

Another factor influencing soil hydraulic conductivity and not considered in its modeling is the pore systems' swelling-shrinkage processes and coinciding pore rigidity. The recent review of literature by Horn *et al.* (2025) showed that when shrinkage and the pore rigidity limit (of -100 hPa) are incorporated, the calculated unsaturated hydraulic conductivity curves (using the van Genuchten model) are generally much flatter and run parallel vs. the measured ones without considering shrinkage. Strengthening the pore system following drying and shrinkage is attributed to more particle contact areas and a less developed aggregation.

4.3. Possible mechanisms of the hydraulic properties changes and further studies

The results of this study showed that biochar effects on the hydraulic properties largely depend on soil texture and the type of biochar. Response of hydraulic properties to biochar application in coarse-textured soils can be attributed to infilling the pores between the sand particles by biochar, leading to reduced inter-granular pore size (Chen *et al.*, 2018). In fine-textured soils vs. coarse-textured soil, biochar addition can affect the hydraulic properties by commonly greater organic matter content and resulting in greater surface areas (Lei and Zhang, 2013). Other mechanisms can be linked with reduced sorptivity and associated water absorption rate of biochar amended soils, resulting in lower hydraulic conductivity (Faloye *et al.*, 2022). Further studies intended of the interactions between pore structure in biochar-soil mixtures using X-ray CT imaging and direct measurements of pore throat lengths and tortuosities depending on soil texture matric potential range, and changes in soil volume will help to improve the performance of hydraulic conductivity models including the statistical-physical model used in this study.

5. SUMMARY AND CONCLUSIONS

The data on soil water retention in response to biochars obtained from woodchips, rice straw and dairy manure at different pyrolysis temperatures applied to sandy and loamy soils in Chinese experiments were used to predict hydraulic conductivity, volumes of variously sized capillaries (from 360.4 to 0.24 μm radius), and equivalent capillary length using the statistical-physical model. The addition of biochars decreased the hydraulic conductivity of the sandy soil in the wet range of matric potential (from saturation to -70 cm H_2O) and increased it at a drier range of potential (from -500 to -15000 cm H_2O). In turn, the conductivity in the loamy soil increased in the biochar-amended plots across the whole matric potential range. At field water capacity, the conductivity increased in all biochar treatments to

around 8% in the sandy soil and 80% in the loamy soil. The biochars derived from the rice straw had the largest effect on the hydraulic conductivity in sandy soil and woodchips in loamy soil. In the majority of cases, the volume of capillaries in the biochar-amended sandy soil increased. In contrast, the volume of larger capillaries in the loamy soil decreased, and smaller capillaries with a 0.53 μm radius increased from 10 to 185%, depending on the biochar type. All biochars generally decreased the equivalent capillary length in the sandy soil and increased its value in the loamy soil. The suitability of the statistical-physical model to predict the hydraulic properties observed in this study and its good predictability of thermal conductivity, electrical conductivity, and gaseous diffusivity reported in previous studies extend the model's capability to assess different soil conductivities under the same experiment.

Author contributions: B. Usowicz: Conceptualization, Investigation, Software, Writing – review and editing. J. Lipiec: Conceptualization, Formal analysis, Methodology, Writing – original draft.

Conflicts of Interest: The authors declare no competing interests.

6. REFERENCES

- Aldrees, A., Nachabe, M., 2019. Capillary length and field capacity in draining soil profiles. *Water Res. Res.* 55, 4499-4507. <https://doi.org/10.1029/2018WR024288>
- Ajayi, A.E., Holthausen, D., Horn, R., 2016. Changes in micro-structural behaviour and hydraulic functions of biochar amended soils. *Soil Till. Res.* 155, 166-175.
- Arya, L.M., Leij, F.J., Shouse, P.J., Van Genuchten, M.Th., 1999. Relationship between the hydraulic conductivity function and the particle size distribution. *Soil Sci. Soc. Am. J.* 63, 1063-1070.
- Azadmard B., Mosaddeghi M.R., Ayoubi S., Chavoshi E., Raoof M., 2018. Spatial variability of near-saturated soil hydraulic properties in Moghan plain, North-Western Iran. *Arabian J. Geosci.* 11(16), 452.
- Azadmard B., Mosaddeghi M.R., Ayoubi S., Chavoshi E., Raoof M., 2020. HYPERLINK "javascript:void(0)" Estimation of near-saturated soil hydraulic properties using hybrid genetic algorithm-artificial neural network. *Ecohydrology Hydrobiology* 20(3), 437-449.
- Blanco-Canqui, H., 2017. Biochar and soil physical properties. *Soil Sci. Soc. Am. J.* 81, 687-47 711. <https://doi.org/10.2136/sssaj2017.01.0017>
- Barnes, R.T., Gallagher, M.E., Masiello, C.A., Liu, Z., Dugan, B., 2014. Biochar-induced changes in soil hydraulic conductivity and dissolved nutrient fluxes constrained by laboratory experiments. *PLoS ONE* 9(9): e108340. <https://doi.org/10.1371/journal.pone.0108340>
- Brooks, R.H., Corey, A.T., 1964. Hydraulic properties of porous media. *Hydrology papers*. Colorado State University, Fort Collins, Colorado 3, 1-27.
- Chen, M., Alim, N., Zhang, Y., Xu, N., Cao, X., 2018. Contrasting effects of biochar nanoparticles on the retention and transport of phosphorus in acidic and alkaline soils. *Environ. Pollut.* 239, 562 570. <https://doi.org/10.1016/j.envpol.2018.04.050>

- Chen, X., Duan, M., Zhou, B., Cui, L., 2022. Effects of biochar nanoparticles as a soil amendment on the structure and hydraulic characteristics of a sandy loam soil. *Soil Use Manag.* 38, 836-849. <https://doi.org/10.1111/sum.12740>
- Chen, Z., Kamchoom, V., Chen, R., Prasittisopin, L., 2023. Investigating the impacts of biochar amendment and soil compaction on unsaturated hydraulic properties of silty sand. *Agronomy* 13, 1845. <https://doi.org/10.3390/agronomy13071845>
- Eadie, W.T., Drijard, D., James, F.E., Roos, M., Sadoulet, B., 1971. *Statistical Methods in Experimental Physics*. North-Holland, Amsterdam, 269-271.
- Edeh, I.G., Mašek, O., Buss, W., 2020. A meta-analysis on biochar's effects on soil water properties – New insights and future research challenges. *Sci. Total Environ.* 714, 136857. <https://doi.org/10.1016/j.scitotenv.2020.136857>
- Edeh, I.G., Mašek, O., 2022. The role of biochar particle size and hydrophobicity in improving soil hydraulic properties. *Eur. J. Soil Sci.* 73(1), e13138. <https://doi.org/10.1111/ejss.13138>
- Faloye, O.T., Ajayi, A.E., Ajiboye, Y., Alatise, M.O., Ewulo, B.S., Adeosun, S.S., *et al.*, 2022. Unsaturated hydraulic conductivity prediction using artificial intelligence and multiple linear regression models in biochar amended sandy clay loam soil. *J. Soil Sci. Plant Nutr.* 22, 1589-1603. <https://doi.org/10.1007/s42729-021-00756-x>
- Faloye, O.T., Ajayi, E.B., Rostek, J., Schroeren, V., Fashina, T.B.A., Horn, R., 2024. Hydraulic and pore functions of differently textured soils modified by biochar from different parts of the mango plant. *Soil Till. Res.* 236, 105944. <https://doi.org/10.1016/j.still.2023.105944>
- Feizi, Z., Ayoubi, S., Mosaddeghi, M.R., Besalatpour, A.A., Zeraatpisheh, M., Rodrigo-Comino, J., 2019. A wind tunnel experiment to investigate the effect of polyvinyl acetate, biochar, and bentonite on wind erosion control. *Archives Agronomy Soil Sci.* 65(8), 1049-1062. <https://doi.org/10.1080/03650340.2018.1548765>
- Feng, J., Shang, M., Liu, P., 2009. Comparative study on the soil water retention curve between macroporous soil and homogeneous soil (in Chinese). *Chin. J. Soil Sci.* 40, 1006-1009.
- Fišarová, L., Berchová, K., Lukáč, M., Beesley, L., Vosátka, M., Hausenblas, M., *et al.*, 2024. Microgranular biochar improves soil fertility and mycorrhization in crop systems. *Soil Use Manag.* 40, 2. <https://doi.org/10.1111/sum.13068>
- Fornes, F., Lidón, A., Belda, R.M., Macan, G.P.F., Cayuela, M.L., Sánchez-García, M., *et al.*, 2024. Soil fertility and plant nutrition in an organic olive orchard after 5 years of amendment with compost, biochar or their blend. *Sci. Rep.* 14(1), 16606. <https://doi.org/10.1038/s41598-024-67565-x>
- Gao, S., DeLuca, T.H., 2022. Rangeland application of biochar and rotational grazing interact to influence soil and plant nutrient dynamics. *Geoderma* 408, 115572. <https://doi.org/10.1016/j.geoderma.2021.115572>
- Garg, A., Zhu H.H., Sarmah, A.K., Mei, G., Gadi, V.K., 2023. Evaluating mechanism and inconsistencies in hydraulic conductivity of unsaturated soil using newly proposed biochar conductivity factor. *Biochar* 5, 34. <https://doi.org/10.1007/s42773-023-00233-x>
- Gliński, J., Lipiec, J., 2018. *Soil Physical Conditions and Plant Roots* 1st Edition, CRC Press, 260pp, First Published 1990. Reissued 2018 by CRC Press Taylor Francis Group ISBN 13: 978-1-351-07670-8 (ebk).
- Global Biochar Market Report 2023 by International Biochar Initiative, US Biochar Initiative is licensed under CC BY-NC-ND 4.0.
- Głąb, T., Palmowska, J., Zaleski, T., Gondek, K., 2016. Effect of biochar application on soil hydrological properties and physical quality of sandy soil. *Geoderma* 28, 11-20. <https://doi.org/10.1016/j.geoderma.2016.06.028>
- Gong, H., Tan, Z., Zhang, L., Huang, Q., 2019. Preparation of biochar with high absorbability and its nutrient adsorption-desorption behaviour. *Sci. Total Environ.* 694. <http://doi.org/10.1016/j.scito.tenv.2019.133728>
- Hessel, R., Wyseure, G., Panagea, I.S., Alaoui, A., Reed, M.S., van Delden, H., *et al.*, 2022. Soil-improving cropping systems for sustainable and profitable farming in Europe. *Land* 11, 780. <https://doi.org/10.3390/land11060780>
- Horn, R., Fleige, H., Dörner, J., Zimmermann, I., Wendroth, O., 2025. Pore rigidity as an undervalued process in soil structure development. *Soil Till. Res.* 245, 106280. <https://doi.org/10.1016/j.still.2024.106280>
- Hyväluoma, J., Kulju, S., Hannula, M., Wikberg, H., Källi, A., Rasa, K., 2018. Quantitative characterization of pore structure of several biochars with 3D imaging. *Environ. Sci. Pollut. Res.* 25, 25648-25658. <https://doi.org/10.1007/s11356-017-8823-x>
- Juriga, M., Šimanský, V., 2018. Effect of biochar on soil structure – review. *Acta fytotechn.* 147. *Zootech.* 21, 11-19. <https://doi.org/10.15414/afz.2018.21>
- Kameyama, K., Miyamoto, T., Iwata, Y., 2019. The preliminary study of water-retention related properties of biochar produced from various. *Materials* 12(1732), 1-13.
- Kaźmierowski, C., 2015. Estimation of the hydraulic properties of soils in the Polish Lowlands (in Polish). *Wydanie I, Poznań: Wydawnictwo Naukowe UAM*, 220.
- Kelishadi, H., Mosaddeghi M.R., Hajabbasi M.A., Ayoubi S., 2014. Near-saturated soil hydraulic properties as influenced by land use management systems in Koohrang region of central Zagros, Iran. *Geoderma* 213, 426-434. <https://doi.org/10.1016/j.geoderma.2013.08.008>
- Kinney, T.J., Masiello, C.A., Dugan, B., Hockaday, W.C., Dean, M.R., Zygourakis K., *et al.*, 2012. Hydrologic properties of biochars produced at different temperatures. *Biomass Bioenergy* 41, 34-43. <https://doi.org/10.1016/j.biombioe.2012.01.033>
- Kirkham, M.B., 2005. *Principles of Soil and Plant Water Relations*. Boston: Elsevier Academic Press.
- Klute, A. (Ed.), 1986. Water retention: laboratory methods. In: *Methods of soil analysis. Part 1. Physical and mineralogical methods*. Am. Soc. Agronomy, Madison, WI, 635-685. <https://doi.org/10.2136/sssabookser5.1.2ed>
- Kroes, J., Supit, I., van Dam, J., van Walsum, P., Mulder, M., 2018. Impact of capillary rise and recirculation on simulated crop yields. *Hydrol. Earth Syst. Sci.* 22, 2937-2952. <https://doi.org/10.5194/hess-22-2937-2018>
- Krzyszczak, J., Baranowski, P., Pastuszka-Woźniak, J., Wesołowska, M., Cymerman, J., Sławiński, C., *et al.*, 2023. Assessment of soil water retention characteristics based on VNIR/SWIR hyperspectral imaging of soil surface, *Soil Till. Res.* 233, 105789. <https://doi.org/10.1016/j.still.2023.105789>
- Kumar, A., Bhattacharya, T., Mukherjee, S., Sarkar, B., 2022. A perspective on biochar for repairing damages in the soil

- plant system caused by climate change-driven extreme weather events. *Biochar* 4, 22. <https://doi.org/10.1007/s42773-022-00148-z>
- Kumar, A., Bhattacharya, T., Shaikh, W.A., Roy, A., Chakraborty, S., Vithanage, M., *et al.*, 2023. Multifaceted applications of biochar in environmental management: a bibliometric profile. *Biochar* 5, 11, <https://doi.org/10.1007/s42773-023-00207-z>
- Lehmann, J., 2007. Bio-energy in the black. *Front. Ecol. Environ.* 5, 381-387. [https://doi.org/10.1890/1540-9295\(2007\)5\[381:BITB\]2.0.CO;2](https://doi.org/10.1890/1540-9295(2007)5[381:BITB]2.0.CO;2)
- Lei, O., Zhang, R., 2013. Effects of biochars derived from different feedstocks and pyrolysis temperatures on soil physical and hydraulic properties. *J. Soils Sediments* 13, 1561-1572. <https://doi.org/10.1007/s11368-013-0738-7>
- Li, Y., Feng, G., Tewolde, H., 2023. Biochar derived from papermill factories improves soil physical and hydraulic properties in no-till cotton fields *Biochar* 5, 35. <https://doi.org/10.1007/s42773-023-00235-9>
- Li, X., Wu, D., Liu, X., Huang, Y., Cai, A., Xu, H., *et al.*, 2024. A global dataset of biochar application effects on crop yield, soil properties, and greenhouse gas emissions. *Sci Data* 11, 57. <https://doi.org/10.1038/s41597-023-02867-9>
- Lim, T.J., Spokas, K., Feyereisen, G., Novak, J., 2015. Predicting the impact of biochar additions on soil hydraulic properties. *Chemosphere* 142. <https://doi.org/10.1016/j.chemosphere.2015.06.069>
- Lipiec, J., Usowicz, B., Kłopotek, J., Turski, M., Frąc, M., 2021. Effects of application of recycled chicken manure and spent mushroom substrate on organic matter, acidity, and hydraulic properties of sandy soils. *Materials* 14, 4036. <https://doi.org/10.3390/ma14144036>
- Liu, Z., Dugan, B., Masiello, C.A., Gonnermann, H.M., 2017. Biochar particle size, shape, and porosity act together to influence soil water properties. *PLoS One* 12, 1-19. <https://doi.org/10.1371/journal.pone.0179079>
- Mualem, Y., 1976. A new model for predicting the hydraulic conductivity of unsaturated porous media. *Water Res. Res.* 12, 513-522. <https://doi.org/10.1029/WR012i003p00513>
- Nemes, A., Schaap, M., Leij, F., Wösten, J., 2001. Description of the unsaturated soil hydraulic database UNSODA version 2.0. *J. Hydrol.* 251, 151-162. [https://doi.org/10.1016/S0022-1694\(01\)00465-6](https://doi.org/10.1016/S0022-1694(01)00465-6)
- Novak, J., Sigua, G., Watts, D., Cantrell, K., Shumaker, P., Szogi, A., *et al.*, 2016. Biochars impact on water infiltration and water quality through a compacted subsoil layer. *Chemosphere* 142, 160-167. <https://doi.org/10.1016/j.chemosphere.2015.06.038>
- O'Keefe, A.O., Brooks, E., Dunkel, C., Shrestha, D.S., 2023. Soil moisture routing modeling of targeted biochar amendment in undulating topographies: an analysis of biochar's effects on streamflow. *AIMS Environ. Sci.* 10, 529-546. <https://doi.org/10.3934/environsci.2023030>
- Orzechowski, M., Smółczyński, S., Długosz, J., Kalisz, B., 2022. Spatial variability of water properties of soils formed from glaciolimnic deposits in Sępólno Lowland (Poland) – results from a field-scale study. *J. Elem.* 27(3): 533-544. <https://doi.org/10.5601/jelem.2022.27.3.2279>
- Saeidi, T., Mosaddeghi M.R., Afyuni M., Ayoubi S., Sauer D., 2023. Modeling the effect of slope aspect on temporal variation of soil water content and matric potential using different approaches by HYDRUS-1D. *Geoderma Regional* 35, e00724. <https://doi.org/10.1016/j.geodrs.2023.e00724>
- Sohi, S., Lopez-Capel, E., Krull, E., Bol, R., 2009. Biochar, climate change and soil: a review to guide future research. *Civ. Eng.* 6618:64. <https://doi.org/10.1139/Z03-132>
- Suliman W., Hars, J.B., Abu-Lail, N.I., Fortuna, A.M., Dallmeyer I., Garcia-Perez M., 2017. The role of biochar porosity and surface functionality in augmenting hydrologic properties of a sandy soil. *Sci. Total Environ.* 574, 139-147. <https://doi.org/10.1016/j.scitotenv.2016.09.025>
- Tomczyk, A., Sokołowska, Z., Boguta, P., 2020. Biochar physico-chemical properties: pyrolysis temperature and feedstock kind effects. *Rev. Env.Sci. Biotechnol.* 19, 191-215. <https://doi.org/10.1007/s11157-020-09523-3>
- Usowicz, B., 2000. Statistical and physical models of mass and energy flow in a porous medium (in Polish). *Acta Agrophys.* 29, 3-113.
- Usowicz, B., 2001. Statistical approach for hydraulic conductivity of porous medium (in Polish). *Acta Agrophys.* 53, 177-187.
- Usowicz, B., Lipiec, J., 2020. Modelling the saturated hydraulic conductivity of soils amended with different biochars. 22nd EGU General Assembly, 4-8 May 2020, id 7575. <https://doi.org/10.5194/egusphere-egu2020-7575>
- Usowicz, B., Lipiec, J., Ferrero, A., 2006a. Prediction of soil thermal conductivity based on penetration resistance and water content or air-filled porosity. *Int. J. Heat Mass Transf.* 49, 5010-5017. <https://doi.org/10.1016/j.ijheatmasstransfer.2006.05.023>
- Usowicz, B., Lipiec, J., Marczewski, W., Ferrero, A., 2006b. Thermal conductivity modelling of terrestrial soil media – a comparative study. *Planet. Space Sci.* 54, 1086-1095. <https://doi.org/10.1016/j.pss.2006.05.018>
- Usowicz, B., Lipiec, J., Łukowski, M., Marczewski, W., Usowicz, J., 2016. The effect of biochar application on thermal properties and albedo of loess soil under grassland and fallow. *Soil Till Res.* 164, 45-51. <http://dx.doi.org/10.1016/j.still.2016.03.009>
- Usowicz, B., Lipiec, J., Łukowski, M., Bis, Z., Usowicz, J., Latawiec, A.E., 2020. Impact of biochar addition on soil thermal properties: Modelling approach. *Geoderma* 376, 114574. <https://doi.org/10.1016/j.geoderma.2020.114574>
- Usowicz, B., Lipiec, J., Siczek, A., 2024. Fitting the van Genuchten model to the measured hydraulic parameters in soils of different genesis and texture at the regional scale. *Int. Agrophys.* 38, 373-382. <https://doi.org/10.31545/intagr/191380>
- Usowicz, B., Lipiec, J., Usowicz, J.B., Marczewski, W., 2013. Effects of aggregate size on soil thermal conductivity: Comparison of measured and model-predicted data. *Int. J. Heat Mass Transf.* 57, 536-541. <https://doi.org/10.1016/j.ijheatmasstransfer.2012.10.067>
- van Genuchten, M.T., 1980. A closed-form equation for predicting the hydraulic conductivity of unsaturated soils. *Soil Sci. Soc. Am. J.* 4, 892-898. <https://doi.org/10.2136/sssaj1980.03615995004400050002x>
- van Genuchten M., Th., Pachepsky, Y., 2011. Hydraulic Properties of Unsaturated Soils. In: Gliński, J., Horabik, J., Lipiec, J., (Eds), *Encyclopedia of Agrophysics*. Springer Dordrecht, Heidelberg, London, New York, 368-376. https://doi.org/10.1007/978-90-481-3585-1_69

- Villagra-Mendoza, K., Horn, R., 2018a. Effect of biochar addition on hydraulic functions of two textural soils. *Geoderma* 326, 88-95. <https://doi.org/10.1016/j.geoderma.2018.03.021>
- Villagra-Mendoza, K., Horn, R., 2018b. Effect of biochar on the unsaturated hydraulic conductivity of two amended soils. *Int. Agrophys.* 32(3), 373-378. <https://doi.org/10.1515/intag-2017-0025>
- Wang, Z., Sedighi, M., Lea-Langton, A.R., Babaei, M., 2022. Hydraulic behaviour of sand-biochar mixtures in water and waste water treatment applications. *J. Hydrol.* 612, 128220. <https://doi.org/10.1016/j.jhydrol.2022.128222>
- Yan, Y., Akbar Nakhli, S.A., Jin, J., Mills, G., Willson, C.S., Legates D.R., *et al.*, 2021. Predicting the impact of biochar on the saturated hydraulic conductivity of natural and engineered media. *J. Environ. Manag.* 1(295), 113143. <https://doi.org/10.1016/j.jenvman.2021.113143>
- Zhang, A., Bian, R., Pan, G., Cui, L., Hussain, Q., Li, L., *et al.*, 2012. Effects of biochar amendment on soil quality, crop yield and greenhouse gas emission in a Chinese rice paddy: a field study of 2 consecutive rice growing cycles. *Field Crop Res.* 127, 153-160. <https://doi.org/10.1016/j.fcr.2011.11.020>
- Zhang, Y., Gu, K., Li J., Tang, C., Shen, Z., Shi, B., 2020. Effect of biochar on desiccation cracking characteristics of clayey soils. *Geoderma* 364, 114182. <https://doi.org/10.1016/j.geoderma.2020.114182>
- Zhang, L., Jing, Y., Chen, G., Wang, X., Zhang R., 2019. Improvement of physical and hydraulic properties of desert soil with amendment of different biochars. *J. Soils Sediments* 19, 2984-2996. <https://doi.org/10.1007/s11368-019-02293-8>